

# The Application of Dual-Layer, Mussel-Inspired, Antifouling Polyglycerol-Based Coatings in Ventricular Assist Devices


Michaël W. Kulka, Sarah Smatty, Felix Hehnen, Tim Bierewirtz, Kim Silberreis, Chuanxiong Nie, Yannic Kerkhoff, Carsten Grötzinger, Sebastian Friedrich, Lars Ingemar Dahms, Jens Dervedde, Ingo Grunwald, Michael Schirner, Ulrich Kertzsch, Klaus Affeld, and Rainer Haag\*

Continuous-flow ventricular assist devices (VADs) have established themselves as a lifesaving therapy option in patients with severe cardiovascular disease. Unfortunately, complications with VADs resulting from the shear-induced formation of surface blood clots are common. In the current work, an antifouling coating based on the combination of mussel-inspired dendritic polyglycerol (MI-dPG) and linear polyglycerol (IPG) is tested for its cell-repelling properties, biocompatibility, and complement activating properties. Furthermore, the adhesion and activation of blood platelets are tested under static and flow conditions. The adhesion and proliferation of two cell types are studied by means of LIVE/DEAD cell staining, and it is clearly observed that the IPG-functionalized MI-dPG coating prevents cell adhesion. Additionally, no cell mortality is observed on all substrates, indicating the biocompatibility of the tested coatings. All coatings show lower (or equal) complement-activating properties than bare titanium, which is considered a highly biocompatible material. Most importantly, the IPG-functionalized system prevents the adhesion and activation of blood platelets under static and flow conditions. Finally, a prototype VAD is successfully coated with MI-dPG under flow conditions. In the current study, the efficient IPG-functionalization of the MI-dPG coating is proved to obtain cell- and platelet-repelling surfaces.

## 1. Introduction

Cardiovascular diseases (CVDs) account for 45% of all deaths, and are the main cause of death for men in all but 12 countries of Europe.<sup>[1,2]</sup> The treatment of patients suffering from CVDs includes lifestyle adaptations (such as quitting smoking and dietary changes), medication for the reduction of low-density lipoprotein cholesterol, cardiac rehabilitation, and surgical interventions (e.g., coronary artery bypass grafting), percutaneous coronary intervention, and the placement of electronic pacemakers or ventricular assist devices (VADs).<sup>[3]</sup> VADs are electromechanical devices for cardiac circulation, which are used to partially or fully replace the function of a failing heart.<sup>[4]</sup> Over the last decades, VADs have established themselves as lifesaving treatment option for patients with refractory heart failure, with a two-year survival rate of 70%.<sup>[5]</sup> The Food and Drug Administrations has approved

M. W. Kulka, Dr. K. Silberreis, C. Nie, Y. Kerkhoff, Prof. M. Schirner, Prof. R. Haag  
 Institute for Chemistry and Biochemistry  
 Freie Universität Berlin  
 Takustraße 3, Berlin 14195, Germany  
 E-mail: haag@chemie.fu-berlin.de  
 S. Smatty, F. Hehnen, T. Bierewirtz, Dr. U. Kertzsch, Prof. K. Affeld  
 Biofluid Mechanics Lab  
 Charité-Universitätsmedizin Berlin  
 Augustenburger Platz 1, Berlin 13353, Germany

 The ORCID identification number(s) for the author(s) of this article can be found under <https://doi.org/10.1002/admi.202000272>.

© 2020 The Authors. Published by Wiley-VCH GmbH. This is an open access article under the terms of the Creative Commons Attribution-NonCommercial-NoDerivs License, which permits use and distribution in any medium, provided the original work is properly cited, the use is non-commercial and no modifications or adaptations are made.

DOI: 10.1002/admi.202000272

Dr. K. Silberreis, Dr. J. Dervedde  
 Institute for Laboratory Medicine  
 Clinical Chemistry and Pathobiochemistry  
 Charité-Universitätsmedizin Berlin  
 Augustenburger Platz 1, Berlin 13353, Germany  
 Dr. C. Grötzinger  
 Department of Hepatology and Gastroenterology  
 Charité-Universitätsmedizin Berlin  
 Augustenburger Platz 1, Berlin 13353, Germany  
 S. Friedrich  
 Process Engineering Department  
 Berlin Heart GmbH  
 Wiesenweg 10, Berlin 12247, Germany  
 Dr. L. I. Dahms  
 Quality Assurance and Regulatory Affairs  
 qtec group GmbH  
 Niels-Bohr-Ring 3–5, Lübeck 23568, Germany  
 Prof. I. Grunwald  
 Department of Industrial and Environmental Biology  
 Hochschule Bremen–City University of Applied Sciences  
 Neustadtswall 30, Bremen 28199, Germany

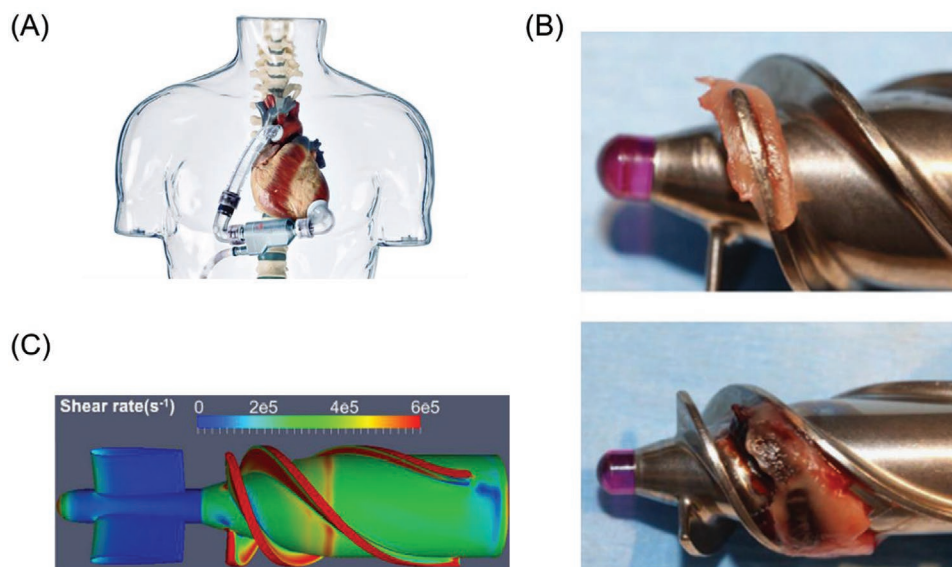


**Figure 1.** A) The INCOR continuous-flow VAD system by Berlin Heart GmbH, which reaches rotation numbers between 5000–10 000 rotations  $\text{min}^{-1}$  ( $2\text{--}9 \text{ l min}^{-1}$ ), leading to shear strain rates up to maximum  $200\,000 \text{ s}^{-1}$ . The production of this specific model of VAD was terminated at the end of 2018. Image kindly provided by Berlin Heart GmbH. B) Examples of thrombosis in the HeartMate II VAD system by Abbott Laboratories (Abbott Park, Illinois, USA). The top image shows a pure fibrin clot resulting from high shear. The bottom images show a fibrin and blood clot (often observed at areas with lower wall shear stress). Reproduced with permission.<sup>[12]</sup> Copyright 2014, Elsevier. C) An in silico modulation of the shear-rates within the HeartMate II VAD.<sup>[13]</sup> The red areas represent the areas with high shear, whereas the yellow, green, and blue areas represent the areas with lower wall shear-stress. The blue part on the left of the image represents a flow straightener.<sup>[13]</sup> The image clearly illustrates the wide variety of shear rates in continuous-flow VAD systems. Reproduced with permission.<sup>[13]</sup> Copyright 2016, Nature Research.

the use of continuous-flow VAD systems.<sup>[6]</sup> However, the use of these systems has its shortcomings: as a result of unspecific protein adhesion and high wall shear rates, the formation of surface blood clots in VADs is common (**Figure 1**).<sup>[7]</sup> The release of these blood clots into the bloodstream constitutes a major risk, as the clots might occlude arteries, effectively blocking the supply of nutrition and oxygen to the downstream tissue. Additionally, the formation of surface blood clots hinders the effectiveness of the VAD system, leading to repeated invasive surgical interventions to clean or fully replace the VAD (i.e., in case of intracorporeal systems). Therefore, the development of durable blood-contacting materials for the prevention of surface blood clots is of major interest for VAD patients.

Commonly, titanium (Ti) (covered with a natural layer of titanium dioxide ( $\text{TiO}_2$ )) and its alloys are used for the production of VADs, resulting from the excellent biocompatibility and low costs of these materials.<sup>[8]</sup> However, the application of these materials is far from ideal with respect to their hemocompatibility. Additionally, it seems that the potential for alternative hemocompatible bulk biomaterials has been largely explored.<sup>[8]</sup> Consequently, scientists have shifted their attention towards surface coatings and surface engineering for the reduction of biomaterial-induced thrombosis. A wide variety of antithrombogenic coating materials has been developed, and the use of coatings has proven itself as a useful strategy for the reduction of biomaterial-induced thrombosis in VADs. In general, VAD coatings can be divided into bioactive coatings and inorganic/organic bioinert coatings.<sup>[8,9,10]</sup> Alternatively, the use of endothelial cell linings for the reduction of biomaterial-induced thrombosis has also been investigated.<sup>[11]</sup>

The immobilization of the bioactive anticoagulant heparin (i.e., an active biomolecule) has been widely reported in scientific literature,<sup>[14]</sup> and the use of this tactic has led to a variety of commercial systems, such as the CARMEDA BioActive Surface (W.L. Gore & Associates) and the Hepamed Heparin Coating (Medtronic plc).<sup>[15]</sup> When inorganic bioinert coatings are discussed, titanium nitride coatings and diamond like carbon coatings are often considered as the current standard.<sup>[8]</sup> An alternative to bioactive antithrombogenic coatings and inorganic bioinert coatings are polymeric antifouling surfaces,<sup>[16]</sup> which effectively prevent the initial adhesion of circulatory proteins and cells, thus lowering the inherent thrombogenicity of the surface. Polyethylene glycol (PEG) has classically been applied as antifouling polymer,<sup>[17]</sup> but suffers from issues considering instability upon heating in air, and immunological recognition upon repeated exposure.<sup>[18]</sup> Additionally, a publication by Kizhakkedathu and co-workers showed that high molecular weight PEG may induce severe red blood cell aggregation, cell toxicity, and dose dependent activation of the blood coagulation, platelets, and complement system.<sup>[19]</sup> Therefore, there is a need for the development of novel polymeric materials which exhibit similar or superior antifouling properties as PEGylated surface, while showing higher thermal stability, oxidative stability, and biocompatibility under physiological conditions. Recently, polyglycerol has emerged as an alternative to PEG with higher oxidative stability and hemocompatibility.<sup>[19,20]</sup>

Polymeric substances can be linked to the surface of blood contacting materials via a wide variety of methods. Traditionally, thiol and siloxane chemistries are applied to modify noble metals and hydroxylated surfaces,<sup>[21]</sup> respectively. Alternatively,

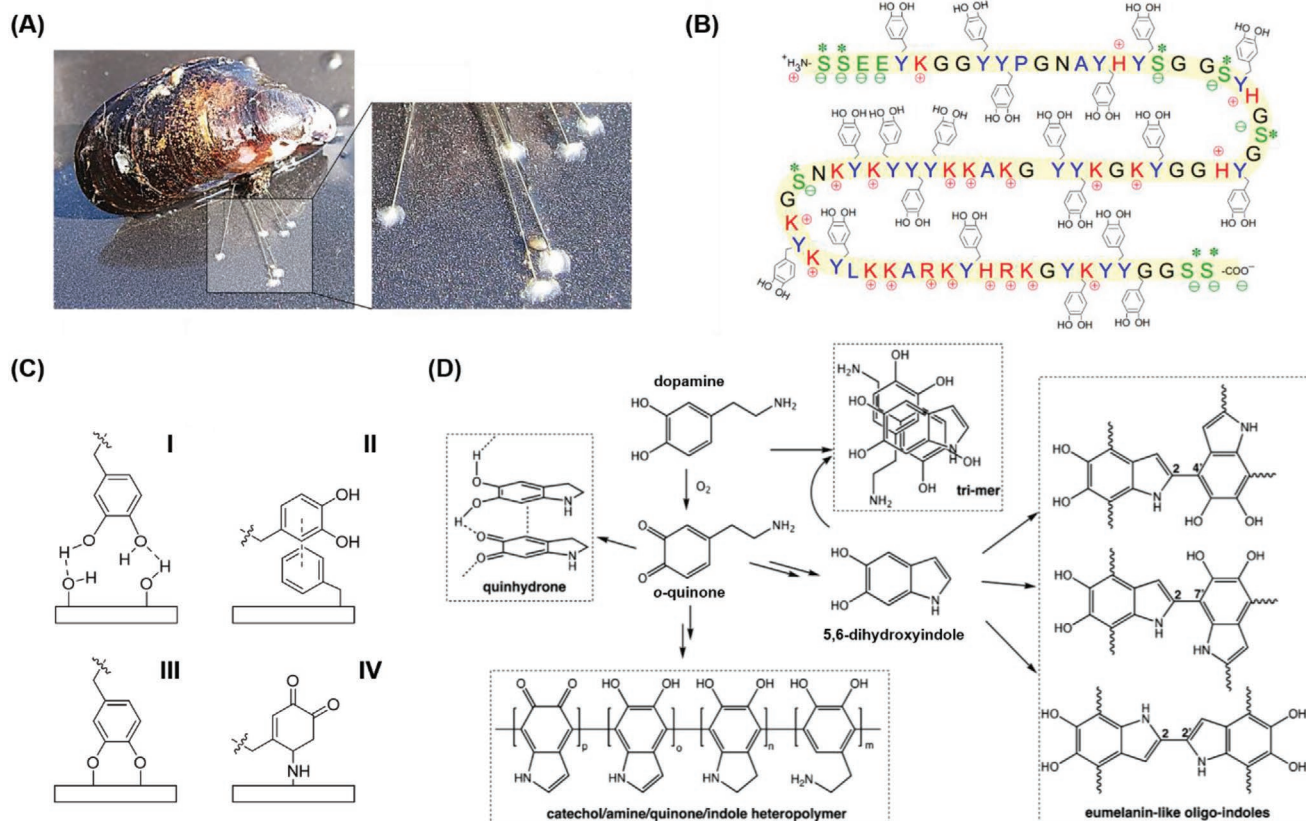


**Figure 2.** A) Adhesion of *Mytilus edulis* via multiple byssal threads. The enlargement on the right shows the adhesive plaque (the white structure) in more detail. B) Schematic representation of the protein sequence of adhesion-mediating mfp-5 of *Mytilus edulis* (Y = DOPA, K = Lysine, S = Serine, and G = Glycine). Reproduced with permission.<sup>[26]</sup> Copyright 2017, The Company of Biologists Ltd. C) Catechols can adhere to a wide variety of substrates via the formation of I) hydrogen-bonds, II)  $\pi$ - $\pi$  stacking, III) the formation of complex-structures, and IV) the formation of Michael adducts.<sup>[26]</sup> D) A summary of the proposed mechanisms for the formation of PDA. For a detailed review on the polymerization of dopamine, the reader is referred to the cited literature. Adapted with permission.<sup>[33,34]</sup> Copyright 2013, American Chemical Society; and Copyright 2012, Wiley-VCH, respectively.

methods such as Langmuir–Blodgett deposition,<sup>[22]</sup> layer-by-layer assembly,<sup>[23]</sup> irradiation-mediated grafting,<sup>[24]</sup> and electrostatic or hydrophobic adsorption can be utilized for the effective immobilization of functional polymers on a surface.<sup>[25]</sup> However, most of these methods require specific chemical and/or physical properties of the substrate or the use of complex machinery, thus limiting their application. Therefore, there is a need for novel facile coating methods that can extend the application of polymeric coatings to the blood-contacting materials that are hard to modify with the current methods.

An interesting alternative for the surface immobilization of polymeric substances is the use of mussel-inspired surface chemistry. Mussels can adhere to virtually every type of substrate, including substrates that are classically defined as nonadhesive (e.g., perfluorinated surfaces).<sup>[26]</sup> Mussels tether themselves to the surface via so-called byssal threads. At the end of these byssal threads, a mixture of mussel foot proteins (mfps) is excreted in the form of an adhesive plaque (Figure 2).<sup>[26]</sup> This adhesive plaque effectively glues the byssal thread to the substrate, hereby fixing the mussel to the surface (even under wet conditions). A publication by Waite et al. showed the high prevalence of lysine- and 3,4-di-hydroxy-phenylalanine (DOPA) amino acids in the mfps that are excreted close to the

plaque–substrate interface (i.e., mainly mfp-3 and mfp-5).<sup>[26]</sup> DOPA and lysine amino acids contain amine- and catechol-functional groups, respectively. Consequently, Waite et al. hypothesized the importance of the catechol functional group in the substrate-independent adhesion characteristics of mfp-3 and -5.<sup>[27]</sup> Later works showed the surface-binding of catechol functional groups via a broad range of reversible noncovalent interactions, including the formation of hydrogen bonds,  $\pi$ - $\pi$  stacking, and the formation of strong but reversible complexes with metal oxides (Figure 2).<sup>[28]</sup> The tethering of catechols to metal oxides via the formation of complex structures was found to be exceptionally strong for Ti substrates ( $\approx 800$  pN).<sup>[29]</sup> The oxidation of catechols leads to the formation of *o*-quinones, which readily react with nucleophiles such as amines and/or thiols to give the respective Michael adducts or Schiff bases. Therefore, the presence of surface-bound amines or thiols leads to the irreversible binding of catechols via the formation of covalent bonds.<sup>[28,29]</sup>

In 2007, Messersmith and co-workers hypothesized that the coexistence of the amine- and catechol-functional groups might contribute to the rapid adhesion of mussels to the substrate.<sup>[30]</sup> Therefore, they selected dopamine as a small molecule containing both functionalities. When dopamine-containing



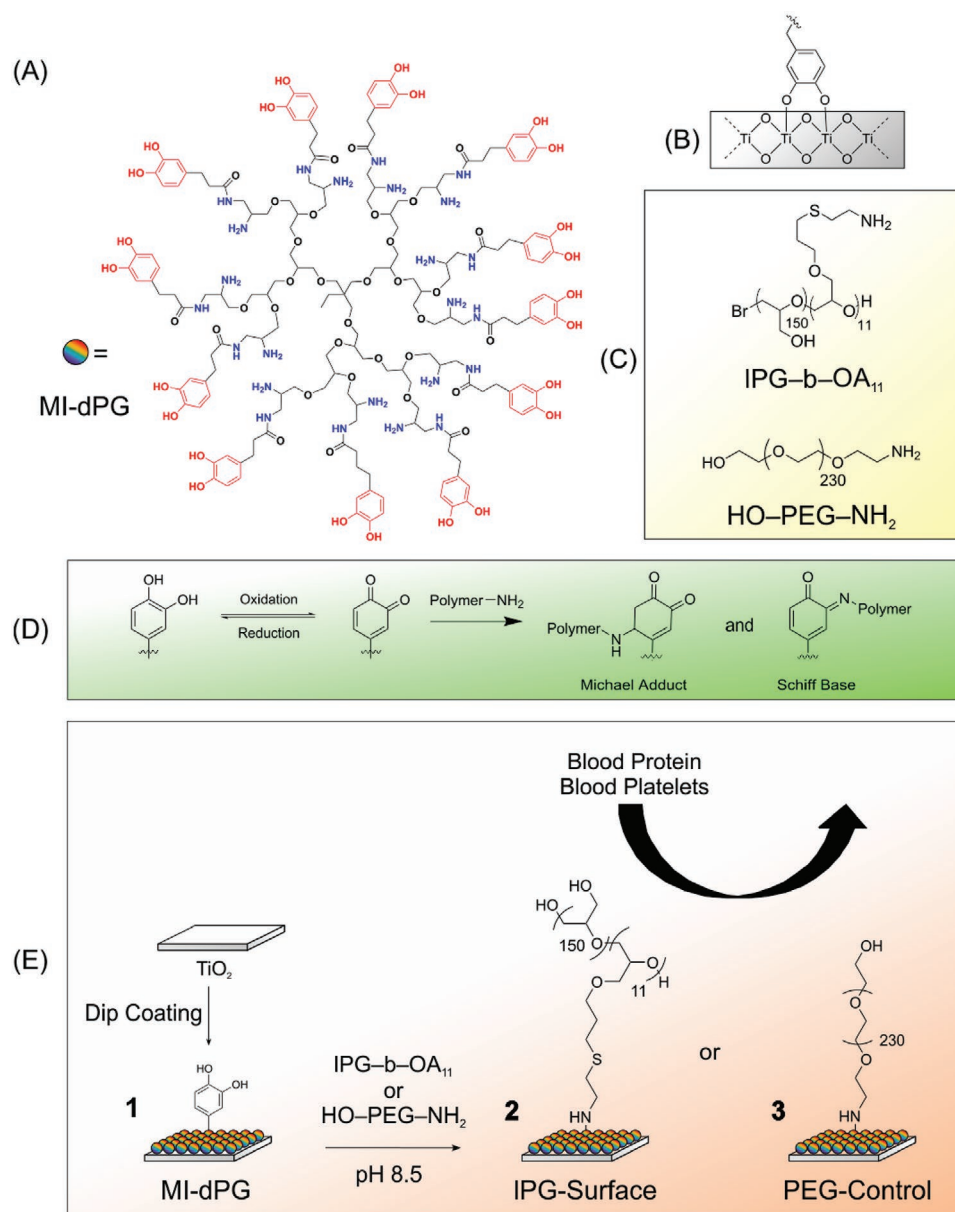


**Figure 3.** A) The molecular structure of MI-dPG. The shown structure is an idealized molecular structure; the amount of the glycerol monomers in the core (in black) varies with the size of the polymer. The dPG-core size used in this work: Mn: 12 kDa and PDI: 1.3. Furthermore, the dPG-core shows up to 60% of branching.<sup>[39]</sup> B) The proposed coordination for the binding of the catechol moieties to the  $\text{TiO}_2$ -surface.<sup>[40]</sup> C) The molecular structure of IPG-*b*-OA<sub>11</sub> and HO-PEG-NH<sub>2</sub>. D) Catechols readily react with amine- (and/or thiol-) functionalized polymers, giving the Schiff-base and Michael addition products. Via the depicted chemistry, the MI-dPG coating was crosslinked and post-functionalized with IPG-*b*-OA<sub>11</sub> or HO-PEG-NH<sub>2</sub> to give surfaces 2 or 3, respectively. E) A schematic display of the functional surfaces 1, 2, and 3.

solutions were buffered to a slightly basic pH (as commonly found in marine environments) the spontaneous formation of polydopamine (PDA) coatings was observed (Figure 2).<sup>[30]</sup> The PDA coatings were found to form on a wide variety of substrates, independently from the physical or chemical properties of the surfaces.<sup>[30]</sup> Furthermore, the covalent introduction of amine- or thiol-terminated methoxy-(polyethylene glycol) to these PDA coatings led to the creation of fouling-resistant surfaces.<sup>[30]</sup> Since Messersmith's initial work, the PDA coating has gained wide interest in the biomedical field (e.g., as a platform for bone and tissue engineering, drug delivery, antimicrobial

activity, and patterned cell adhesion).<sup>[31]</sup> However, the initial method for the formation of PDA suffered from slow coating formation and limited coating thickness. Additionally, the PDA coating appears dark brown/black, making it unsuitable for various optical applications.<sup>[30]</sup>

In 2014, Wei et al. developed mussel-inspired dendritic polyglycerol (MI-dPG) (Figure 3), which did not only contain the functional groups that are commonly found in mfps, but also mimicked the size and molecular weight of the mfps.<sup>[35]</sup> Subsequent polymerization of MI-dPG under slightly alkalic oxidizing conditions led to the rapid formation of substrate-independent

coatings with controllable coating thicknesses and roughness (thickness up to 4  $\mu\text{m}$  after 4 h of coating). Additionally, the coating appeared transparent to white, depending on the total thickness of the coating.<sup>[35]</sup> Earlier projects by our group showed the facile postfunctionalization of the MI-dPG coating with nanoparticles and acyl chlorides, for the introduction of tailored surface properties.<sup>[36]</sup> In the current work,  $\text{TiO}_2$  was especially of interest as it is commonly found as the blood contacting material in the interior of VADs.<sup>[8]</sup> We recently demonstrated the successful formation of highly stable antifouling (i.e., protein and cell repelling) coatings via the introduction of an oligo amine-functionalized block-copolymer of linear polyglycerol (IPG-*b*- $\text{OA}_{11}$ , OA = oligo amine) to MI-dPG-coated  $\text{TiO}_2$  substrates (Figure 3).<sup>[37]</sup> It was hypothesized that the application of such an antifouling coating could prevent the primary adhesion of protein from the bloodstream to  $\text{TiO}_2$ . Consequently, the adhesion and subsequent activation of blood platelets could potentially be prevented. Therefore, the application of an IPG-functionalized MI-dPG coating in VAD systems could potentially lower the risk of shear- and biomaterial-induced thrombosis.

The current study is a follow-up work of an earlier project by our group, which showed the facile formation, high stability, and antifouling properties of IPG-*b*- $\text{OA}_{11}$ -functionalized MI-dPG on  $\text{TiO}_2$  (Figure 3).<sup>[37]</sup> The aim of the current work was to investigate the applicability of this antifouling coating with respect to reduce shear- and biomaterial-induced thrombosis on medically relevant  $\text{TiO}_2$ . The IPG-*b*- $\text{OA}_{11}$ -functionalized coating was compared to a control system, in which the MI-dPG coating was functionalized with an amine-terminated hydroxy-polyethylene glycol (HO-PEG-NH<sub>2</sub>). Both linear polymers were of similar molecular weight ( $\approx 10$  kDa), but varied in the amount of surface binding groups (i.e., multivalent surface binding via multiple amine groups for IPG-*b*- $\text{OA}_{11}$  vs monovalent binding via a single amine group for HO-PEG-NH<sub>2</sub>) (Figure 3).<sup>[37]</sup> Initially, the cytotoxicity of the relevant polymers was investigated towards two cell types. Subsequently, the proliferation, adhesion, and viability of these cells were investigated on bare  $\text{TiO}_2$  substrate, the MI-dPG coating, and the MI-dPG coating postfunctionalized with IPG-*b*- $\text{OA}_{11}$  or HO-PEG-NH<sub>2</sub>. Next, the complement activating properties of the various coatings were studied. Most importantly, the adhesion and activation of blood platelets were studied on the various substrates under static and flow conditions. Finally, the applicability of MI-dPG as a coating material for VADs was investigated. A prototype VAD system was coated with MI-dPG under flow conditions, and subsequently the coating was visualized via the immobilization of a commercially available amine-functionalized fluorophore.

## 2. Results and Discussion

The investigated coatings consisted of MI-dPG (surface 1) postfunctionalized with either IPG-*b*- $\text{OA}_{11}$  (surface 2) or HO-PEG-NH<sub>2</sub> (surface 3) (Figure 3). As substrate material, glass coated with a transparent  $\text{TiO}_2$ -layer ( $\approx 30$  nm) was utilized (see Section S1.2. in the Supporting Information). The MI-dPG and IPG-*b*- $\text{OA}_{11}$  polymers were synthesized according to methods that were published earlier by our group.<sup>[37]</sup> In brief, MI-dPG was

synthesized in a four step synthesis, starting from dendritic polyglycerol (dPG). First, 100% of the hydroxyl functional groups of the dPG scaffold were transformed to amines via mesylation, azidation, and subsequent reduction of the azide groups. Next, 40% of these amines were functionalized with catechols (Figure 3).<sup>[36a]</sup> Under basic oxidizing conditions, the MI-dPG polymer can undergo crosslinking reactions via the formation of Michael adducts or Schiff bases between the amine- and catechol-functional groups of adjacent MI-dPG polymers. A previous study by our group showed that the polymerization of MI-dPG leads to the formation of aggregates in solution, which form the MI-dPG coating via a precipitation and aggregation mechanism.<sup>[36a]</sup> The binding of the MI-dPG coating to the substrate occurs through the versatile binding properties of its catechol moieties (Figures 2 and 3). Another study of our group has shown the effective formation of MI-dPG coatings on a broad range of substrates.<sup>[35]</sup> The IPG-*b*- $\text{OA}_{11}$  block-copolymer was synthesized in a three-step synthesis, starting with the synthesis of a block-copolymer of ethoxyethyl glycidyl ether (EEGE) and allyl glycidyl ether (AGE), utilizing a modified version of a method that was earlier published by Gervais et al.<sup>[37,38]</sup> Subsequently, the EEGE-*b*-AGE block-copolymer was acetal deprotected, transforming the EEGE-block to IPG. Finally, the IPG-*b*-AGE polymer was functionalized with amine-functional groups, giving the IPG-*b*- $\text{OA}_{11}$  block-copolymer (Figure 3).<sup>[37]</sup> IPG-*b*- $\text{OA}_{11}$  was subsequently immobilized on the MI-dPG coating utilizing a straight-forward dip-coating procedure under basic oxidizing conditions (i.e., IPG-*b*- $\text{OA}_{11}$  was bound to the MI-dPG coating via the formation of Michael adducts and Schiff bases).<sup>[37]</sup> In addition, a PEG-based control coating was established by incubating the MI-dPG coating with a solution of commercially available HO-PEG-NH<sub>2</sub> (Figure 3).<sup>[37]</sup> For a more detailed description of the synthesis of the IPG-*b*- $\text{OA}_{11}$  and MI-dPG polymers, the formation/stability of the various coatings, and the antifouling characteristics of the IPG-*b*- $\text{OA}_{11}$  functionalized MI-dPG coating, the reader is referred to the cited literature.<sup>[37]</sup>

## 3. Cell Adhesion and Proliferation Tests

The proliferation and adhesion of human alveolar basal epithelial carcinoma cells (A549) and chicken fibroblast cells (DF-1) was investigated on the various coatings, in order to assess the biocompatibility of the substrates to a broad range of cell types. The proliferation of (for the VAD-system more relevant) human umbilical vein endothelial cells (HUVEC) on bare  $\text{TiO}_2$  and surfaces 1, 2, and 3 was studied in detail in an earlier project of our group.<sup>[37]</sup> It is important to notice that the coatings that were studied in this work were developed as blood-contacting materials, i.e., the coatings would not be exposed to any sort of tissue during their application in VAD systems. Nevertheless, it was important that the coatings showed antifouling and cell-repelling properties while not being toxic to (any type of) cells, as the adhesion (and subsequent proliferation) of cells from the bloodstream to the VAD's interior could potentially lead to major complications.

Cell adhesion and proliferation was assessed by directly seeding the cells onto the bare  $\text{TiO}_2$  substrate and surfaces 1, 2,

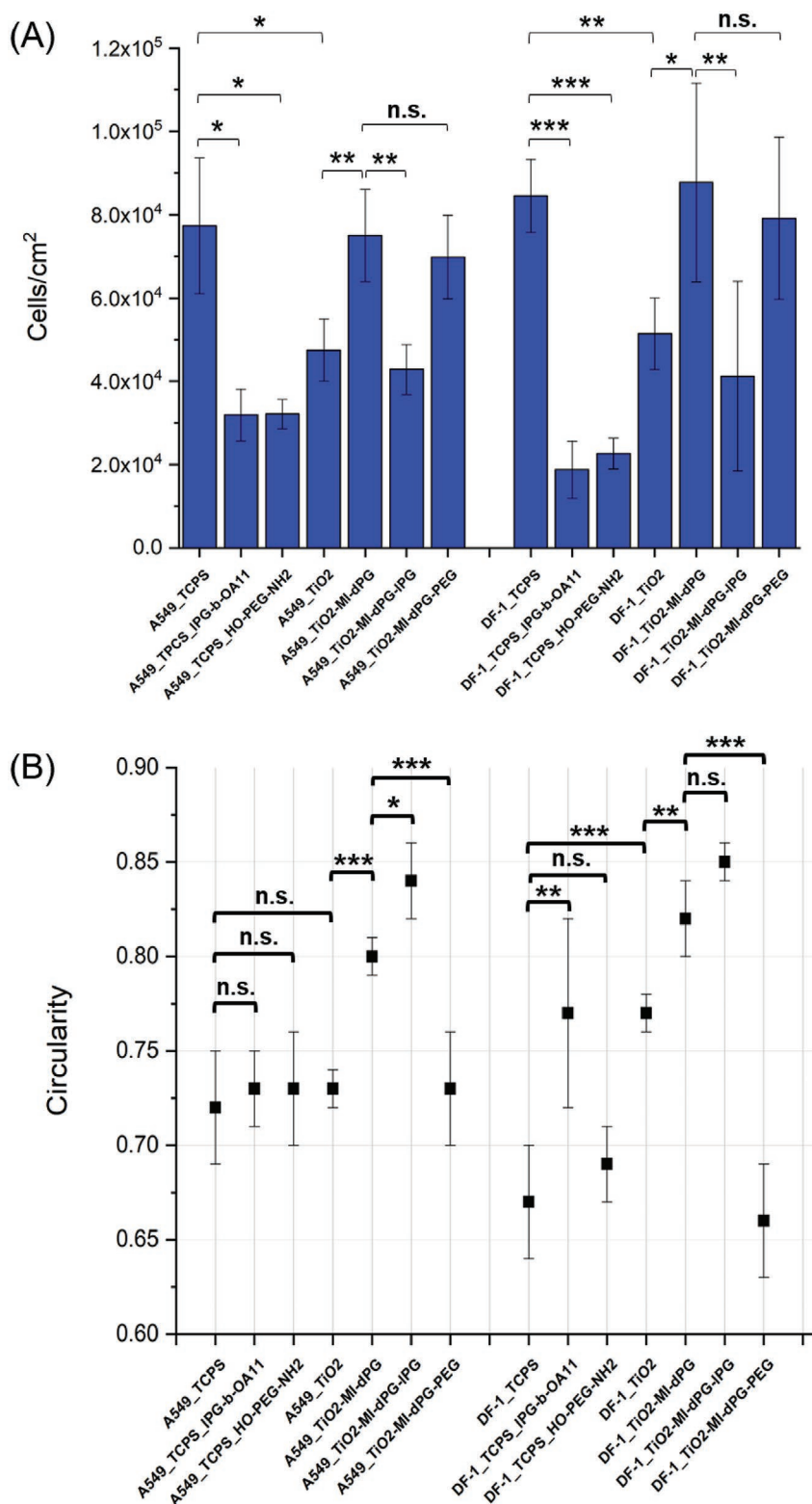


**Figure 4.** A) A graphical representation of the cell numbers on the various coatings. The error bars represent the standard deviation from the mean. The amount of cells was determined from three images per coating type. B) A graphical representation of the circularity of the cells on the various coatings. The circularity was determined from minimal three images per coating type, while analyzing minimal 20 cells per image. For the morphology analysis of the A549 and DF-1 cells on surface 2 and on TCPs incubated with IPG-*b*-OA<sub>11</sub> a minimum of five cells per image was analyzed. The error bars represents the standard deviation from the mean, n.s. = not significant. \**p* ≤ 0.05, \*\**p* ≤ 0.01, \*\*\**p* ≤ 0.001. The *p*-values were calculated utilizing a two-tailed *t*-test under the assumption of equal variance.

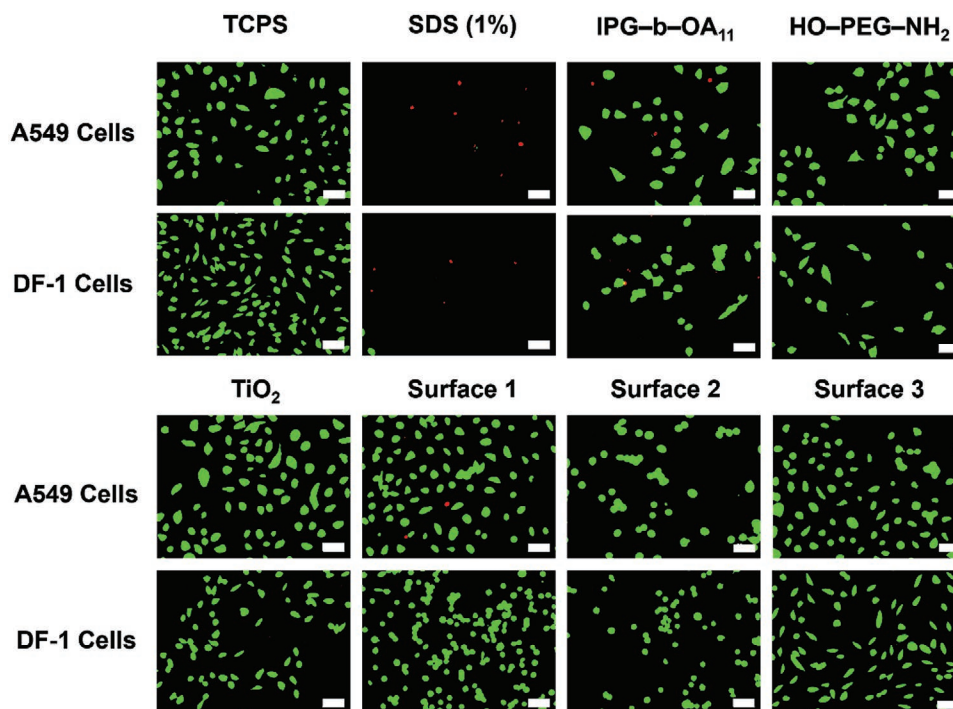


**Figure 5.** LIVE/DEAD Staining of A549 and DF-1 cells on the various substrates. Alive cells appear in green whereas dead cells appear in red. The scale bars represent 50  $\mu\text{m}$ . Incubation of the cells on TCPS showed the normal growth and spreading of live cells, whereas dead cells were observed on TCPS that was incubated with medium that contained 1 wt% sodium dodecyl sulfate (SDS). Incubation with IPG-*b*-OA<sub>11</sub> (10 mg mL<sup>-1</sup>) led to reduced cell viability for the DF-1 cells, whereas incubation with the HO-PEG-NH<sub>2</sub> (10 mg mL<sup>-1</sup>) did not affect the cell viability on the TCPS surface. Furthermore, no reduced cell viability was observed for the A549 and DF-1 cells on the TiO<sub>2</sub> substrate and surfaces 1, 2, and 3.

and 3. After 24 h of culturing, the cells were stained with a commercial LIVE/DEAD cell staining kit. Analysis of the stained cells was achieved utilizing a fluorescence microscope and the Java-based, image-processing program “ImageJ” (the quantification process is described in Figure S1 and Section S1.8 in the Supporting Information). The adhesion and proliferation of the cells were also studied in the presence of high concentrations of the dissolved IPG-*b*-OA<sub>11</sub> and HO-PEG-NH<sub>2</sub> polymers. For this, the A549 and DF-1 cells were cultured on tissue culture polystyrene (TCPS) for 24 h. Subsequently, the cell medium was exchanged for medium containing dissolved IPG-*b*-OA<sub>11</sub> or HO-PEG-NH<sub>2</sub> at 10 mg mL<sup>-1</sup>. After another 24 h of cell culturing, the cells were stained and the cell number, cellular morphology, and overall cell viability were quantified. As a negative control, the cells were incubated with normal cell medium on TCPS. The morphology of the cells was reported as a normalized shape factor that describes the circularity of the adherent cells. Cell circularity is often used as a parameter describing the adhesion of cells: fully circular cells (i.e., cells with a shape factor of 1) do not adhere, whereas spread-out cells (i.e., cells with low shape factors) do adhere to the surface.

On the TCPS control, high cell numbers of both cell types were observed in comparison to the other tested substrates (Figures 4 and 5 and Table S1, Supporting Information). Furthermore, the cells were mainly observed in their spread-out adherent state (Figures 4 and 5 and Table S1, Supporting Information). When the cells were cultured on TCPS in the presence of dissolved IPG-*b*-OA<sub>11</sub>, a significant reduction in the

cell number was observed for both the A549 (59% reduction in respect to TCPS) and DF-1 cells (78% reduction in respect to TCPS) (Figures 4 and 5 and Table S1, Supporting Information). Furthermore, the DF-1 cells showed an increased circularity in respect to the bare TCPS substrate, which indicated that the cells adhered less well to TCPS in the presence of IPG-*b*-OA<sub>11</sub> (Figures 4 and 5 and Table S1, Supporting Information). The A549 cells did only show a minor nonsignificant increase in their circularity, indicating that the adhesion of the cells was only slightly reduced by the presence of IPG-*b*-OA<sub>11</sub> (Figures 4 and 5 and Table S1, Supporting Information). When the cell numbers of the A549 and DF-1 cells were quantified on TCPS in the presence of dissolved HO-PEG-NH<sub>2</sub>, strong reductions in the cell numbers of the A549 (59% reduction in respect to TCPS) and DF-1 cells (73% reduction in respect to TCPS) were observed. However, incubation with HO-PEG-NH<sub>2</sub> did not lead to significant changes in the cell circularities of both cell types, in respect to the bare TCPS substrate (Figures 4 and 5 and Table S1, Supporting Information). The observed reductions in the cell adhesion were explained by the electrostatic binding of the positively charged amines of the IPG-*b*-OA<sub>11</sub> and HO-PEG-NH<sub>2</sub> polymers to the negatively charged TCPS surface,<sup>[41]</sup> which led to the formation of a surface hydration layer that functioned as a physical barrier for the prevention of cell adhesion.<sup>[42]</sup> As a result, reduced cell numbers were observed for TCPS in the presence of dissolved IPG-*b*-OA<sub>11</sub> or HO-PEG-NH<sub>2</sub>. Furthermore, electrostatic immobilization of IPG-*b*-OA<sub>11</sub> on the TCPS substrate led to increased cell circularity for both cell types



(i.e., reduced cell adhesion), which was explained by the antifouling surface properties of the IPG-*b*-OA<sub>11</sub> monolayer.<sup>[16b]</sup> The stability of the IPG-*b*-OA<sub>11</sub> monolayer might have resulted from multivalent electrostatic interactions between the amine groups of the OA-block of IPG-*b*-OA<sub>11</sub> and the TCPS surface. For the TiO<sub>2</sub> substrate, a significant reduction in the cell number was observed in respect to the bare TCPS substrate for both cell types (39% reduction for both cell types) (Figures 4 and 5 and Table S1, Supporting Information). Additionally, the circularity of the DF-1 cells significantly increased in respect to the TCPS substrate. A minor nonsignificant increase in the circularity was observed for the A549 cells on TiO<sub>2</sub> when compared to the TCPS substrate (Figures 4 and 5 and Table S1, Supporting Information). For surface 1, a significant increase in the cell number of both cell types was observed in respect to TiO<sub>2</sub> (58% increase for the A549 cells and 71% increase for the DF-1 cells) (Figures 4 and 5 and Table S1, Supporting Information). Additionally, the circularity of both cell types clearly increased on surface 1 in respect to the bare TiO<sub>2</sub> substrate (Figures 4 and 5 and Table S1, Supporting Information). Although higher cell numbers were observed, analysis of the cell morphology indicated that the cells adhered less well on surface 1 than on the bare TiO<sub>2</sub> substrate, which was explained by the increased hydrophilic character of surface 1 in comparison to bare TiO<sub>2</sub>. For surface 2, a significant decrease in the cell number of both cell types was observed in respect to surface 1 (43% reduction for the A549 cells and 53% reduction for the DF-1 cells) (Figures 4 and 5 and Table S1, Supporting Information). Furthermore, the circularity of both cell types increased on surface 2 in respect to surface 1 (Figures 4 and 5 and Table S1, Supporting Information). The circularity observed for surface 2 was the highest of all investigated substrates, indicating that surface 2 was the most effective coating for the prevention of cell adhesion. The nonadhesion of the cells to surface 2 was in line with an earlier work by our group, which showed the antifouling properties of surface 2.<sup>[37]</sup> The nonadherent behavior of the cells was explained by the formation of a surface hydration layer, which formed a physical barrier that effectively prevented the adhesion of the A549 and DF-1 cells.<sup>[42]</sup> For surface 3, a slight but nonsignificant decrease in the cell number of both cell types was observed in respect to surface 1 (10% reduction for the A549 cells and 7% reduction for the DF-1 cells) (Figures 4 and 5 and Table S1, Supporting Information). Furthermore, the circularity of both cell types clearly decreased on surface 3 in respect to surface 1, indicating improved adhesion of the cells to the surface (Figures 4 and 5 and Table S1, Supporting Information). These results were unexpected, as the introduction of HO-PEG-NH<sub>2</sub> was supposed to introduce antifouling properties to the surface.<sup>[17]</sup> These findings were explained by suboptimal grafting of the HO-PEG-NH<sub>2</sub> polymer to surface 1, as a result from the use of high molecular weight PEG with a single anchoring amine-group.<sup>[37,43]</sup> As a result, the sufficient formation of a stable surface hydration layer might have not occurred, resulting in the adhesion of the A549 and DF-1 cells.<sup>[42]</sup> Further optimization of surface 3 (e.g., optimization of the chain length and surface density of HO-PEG-NH<sub>2</sub>) might lead to coatings with antifouling properties that are superior to those of surface 3. However, optimization of the PEG-based system was beyond the scope of the current investigation.

Next, the cell viability at the surface was investigated via LIVE/DEAD cell staining. The total viability of the adherent cells was determined by dividing the amount of living cells by the total amount of cells that were observed on the surface (Figures 4 and 5 and Table S1, Supporting Information). High cell viability (>95%) was observed in all cases. Only for the DF-1 cells on TCPS in the presence of dissolved IPG-*b*-OA<sub>11</sub> (10 mg mL<sup>-1</sup>) a slightly reduced cell viability (74.1 ± 11.3%) was observed (Figure S4, Supporting Information). This observation was explained by the presence of free amines in the OA-block of IPG-*b*-OA<sub>11</sub>. Similar cytotoxic effects have also been observed for other amine-containing polymeric structures.<sup>[44]</sup> However, it has to be noticed that IPG-*b*-OA<sub>11</sub> in its bound form (i.e., surface 2) did not reduce cell viabilities at the surface for the both cell types (Figure S4 and Table S1, Supporting Information). Besides, no reduced cell viability was observed for the A549 cells on TCPS in the presence of dissolved IPG-*b*-OA<sub>11</sub> (10 mg mL<sup>-1</sup>), indicating that the different cell types were not equally sensitive to IPG-*b*-OA<sub>11</sub>.

#### 4. Cytotoxicity Testing

LIVE/DEAD staining can only quantify toxic effects directly at the surface. Therefore, the concentration-dependent cytotoxicity of dissolved IPG-*b*-OA<sub>11</sub> and HO-PEG-NH<sub>2</sub> was assessed using a commercially available cell counting kit-8 (CCK-8), which is a sensitive colorimetric assay for the quantification of viable cells. The tests were performed by culturing A549 and DF-1 cells for 24 h on TCPS in cell medium that contained the respective polymers at various concentrations (0.08–10 mg mL<sup>-1</sup>). Subsequently, the cell viability in the medium was quantified (Figure S5, Supporting Information). No cytotoxicity (i.e., a cell viability of >80%) was observed in case of the A549 cells for IPG-*b*-OA<sub>11</sub> concentrations up till 5 mg mL<sup>-1</sup> (Figure S5, Supporting Information). However, clearly reduced cell viability (44.2 ± 3.2%) was observed for high IPG-*b*-OA<sub>11</sub> concentrations (10 mg mL<sup>-1</sup>) (Figure S5, Supporting Information). In case of the DF-1 cells, no cytotoxicity was observed up till IPG-*b*-OA<sub>11</sub> concentrations of 2.5 mg mL<sup>-1</sup> (Figure S5, Supporting Information). However, a slightly decreased cell viability was observed for the DF-1 cells at an IPG-*b*-OA<sub>11</sub> concentration of 5 mg mL<sup>-1</sup> (63.0 ± 3.4% viability), and for higher concentrations a further reduction of the cell viability was observed (41.4 ± 5.8% viability for IPG-*b*-OA<sub>11</sub> at 10 mg mL<sup>-1</sup>) (Figure S5, Supporting Information). Again, the reduced cell viability was explained by the presence of free amines in the OA-block of IPG-*b*-OA<sub>11</sub>.<sup>[44]</sup> In contrast, HO-PEG-NH<sub>2</sub> did not show any cytotoxicity in both cell types up to concentrations of 10 mg mL<sup>-1</sup>, which was explained by the biocompatible character of PEG and the low prevalence of free amines in the polymer chains.

An earlier work of our group showed the high stability of surface 2 in both phosphate-buffered saline (PBS) (10 × 10<sup>-3</sup> M, pH 7.4) and aqueous sodium dodecyl sulfate (SDS) (1 wt%) for at least one month at room temperature.<sup>[37]</sup> Besides, only relatively low concentrations of IPG-*b*-OA<sub>11</sub> are required (i.e., 1 mg mL<sup>-1</sup>) for the creation of surface 2 from surface 1. Therefore, it is highly unlikely that surface 2 would release sufficient (if any) IPG-*b*-OA<sub>11</sub> to elevate local concentrations of the unbound



polymer until a point of cytotoxicity. Additionally, after 24 h of cell culturing no cytotoxicity was observed via LIVE/DEAD cell staining in case of surface 2 for both cell lines, furthermore indicating the biocompatibility of the LPG-*b*-OA<sub>11</sub>-functionalized MI-dPG coating. The combined cytotoxicity and cell proliferation/adhesion data showed the biocompatibility of surfaces 1, 2, and 3 and their constituents to the A549 and DF-1 cells. Furthermore, the cell repelling properties of surface 2 were clearly displayed.

#### 4.1. Substrate-Induced Complement Activation

Besides thrombogenicity, blood-related complement activation constitutes another important aspect in blood compatibility.<sup>[14,45]</sup> Therefore, the complement activation was assessed by measuring the level of anaphylatoxin C5a in platelet rich plasma (PRP) that was exposed to the TiO<sub>2</sub> substrate or surfaces 1, 2, or 3, using a commercially available enzyme-linked immunosorbent assay (ELISA). The tests were performed with full Ti substrates (covered with a natural TiO<sub>2</sub>-layer), as glass is known to trigger the activation of the complement system.<sup>[46]</sup> Observations showed slightly lower C5a levels in the PRP-supernatant of surface 3 when compared to surface 2, after 2, 3, 4, and 5 h of incubation. Nevertheless, the C5a levels observed for the PRP on surface 2 were similar (or lower) to the levels observed for the PRP on TiO<sub>2</sub>, at  $t = 3$  h ( $1.50 \pm 0.06$  ng mL<sup>-1</sup> for TiO<sub>2</sub> and  $1.45 \pm 0.08$  ng mL<sup>-1</sup> for surface 2),  $t = 4$  h ( $1.67 \pm 0.05$  ng mL<sup>-1</sup> for TiO<sub>2</sub> and  $1.40 \pm 0.06$  ng mL<sup>-1</sup> for surface 2), and  $t = 5$  h ( $1.61 \pm 0.08$  ng mL<sup>-1</sup> for TiO<sub>2</sub> and  $1.53 \pm 0.09$  ng mL<sup>-1</sup> for surface 2) (Table S2 and Figure S6, Supporting Information). When the C5a levels at  $t = 5$  h of the PRP-supernatant of TiO<sub>2</sub> and surfaces 1, 2, and 3 were compared to PRP in which complement activation was triggered by adding zymosan from *Saccharomyces cerevisiae* (positive control), lower C5a-levels were clearly observed for all substrates (Table S2 and Figure S6, Supporting Information). However, compared to nonactivated PRP (negative control), all substrates showed a slight elevation of the C5a levels (Table S2 and Figure S6, Supporting Information). Still, the results showed only minor variation between the C5a levels in the PRP-supernatant of TiO<sub>2</sub> and surfaces 1, 2, and 3, even after 5 h of incubation, indicating that the coatings showed similar (or even slightly better) complement compatibility as the full Ti substrates (Table S2 and Figure S6, Supporting Information).

#### 4.2. Substrate-Induced Platelet Activation

The thrombogenicity of the biomaterials was assessed by investigating the degree of the platelet deposition on the various substrates and by assessing the morphology of the adherent blood platelets by means of scanning electron microscopy (SEM). As whole blood contains many other types of blood cells, the tests were performed with PRP, which only contains blood platelets and the soluble blood factors. Platelets change their shape from spherical to stellate appearance upon activation (finally resulting in the formation of platelet aggregates), which can be monitored by means of SEM.<sup>[47]</sup> Many investigations have

been focused on biomaterial-induced activation of blood platelets. However, most of these studies did not consider the time-dependent accumulation of pro-thrombogenic protein on the surface of the biomaterial, prior to platelet adhesion and activation. As the long-term fate of the development such a protein corona is hard to determine in vitro, the TiO<sub>2</sub> substrate and surfaces 1, 2, and 3 were incubated with fibrinogen from human plasma (Fib) as a pro-thrombogenic agent, prior to the platelet adhesion experiments. Fib is considered the main protein promoting the adhesion of platelets to biomaterials under low shear conditions.<sup>[48]</sup> In this way, the long-term aggregation of pro-thrombogenic protein on the various substrates was simulated. From now on, the Fib-incubated substrates will be referred to as “surface X (Fib),” whereas the non-Fib-incubated substrates will be denoted as “surface X” (with X = the TiO<sub>2</sub> substrate or surface 1, 2, or 3). Analysis of TiO<sub>2</sub> (Fib) and surface 1 (Fib) clearly showed the formation of large aggregates of activated platelets after 3 h incubation with PRP at 37 °C (Figure 6). In contrast, on surface 2 (Fib) the platelets were mainly found in their inactivated spherical shape, which was explained by the reduced degradation of Fib as a result of the high presence of -OH moieties at the surface.<sup>[48]</sup> Furthermore, the overall number of platelets appeared to be lower on surface 2 (Fib) than on the other surfaces. For surface 3 (Fib), the results varied, and the platelets were found in both activated and inactivated form. Nevertheless, fewer platelets seemed to appear on surface 3 (Fib) than on the TiO<sub>2</sub> substrate and surface 1 (Fib). The overall number of platelets on the surface is often used to indicate the thrombogenicity of the surface.<sup>[49]</sup> However, in this work the platelets merged in their final stage of activation. Therefore, exact platelet quantification was challenging (and therefore considered inaccurate) when performed by SEM.

#### 4.3. Platelet Adhesion in the Stagnation-Point Flow Model

In order to perform in vitro quantitative monitoring of platelet adhesion under variable wall shear conditions, Affeld et al. developed the stagnation-point flow model (Figure S2, Supporting Information).<sup>[7b,50]</sup> The stagnation-point flow model was developed to mimic the blood flow at the bifurcations of larger blood vessels, and therefore it assesses the adhesion of platelets under clinically relevant wall shear rates. The stagnation-point flow model enables visualization of platelet adhesion at wall shear stresses from 0 to 180 1 s<sup>-1</sup> in a single measurement, by using a custom-made flow chamber, a fluorescence-inverted microscope, and blood containing fluorescently labeled platelets (Figure 7). To investigate platelet adhesion to the TiO<sub>2</sub> substrate and surfaces 1, 2, and 3 in the stagnation-point flow model, glass cover slips were coated with a transparent TiO<sub>2</sub> layer by means of PVD (see Section S1.2. in the Supporting Information). Subsequently, these cover slips were functionalized to give surfaces 1, 2, and 3, respectively. Collagen-coated glass substrates were used as positive control to confirm the clotting ability of the blood. Besides, coverslips that were spin-coated with polyurethane (PU) or polydimethylsiloxane (PDMS) were tested as medically relevant reference materials.<sup>[51]</sup> Substrates within one sequence, (i.e., TiO<sub>2</sub>, PU, PDMS, collagen, and surfaces 1, 2, and 3), were always performed with blood originating from the same

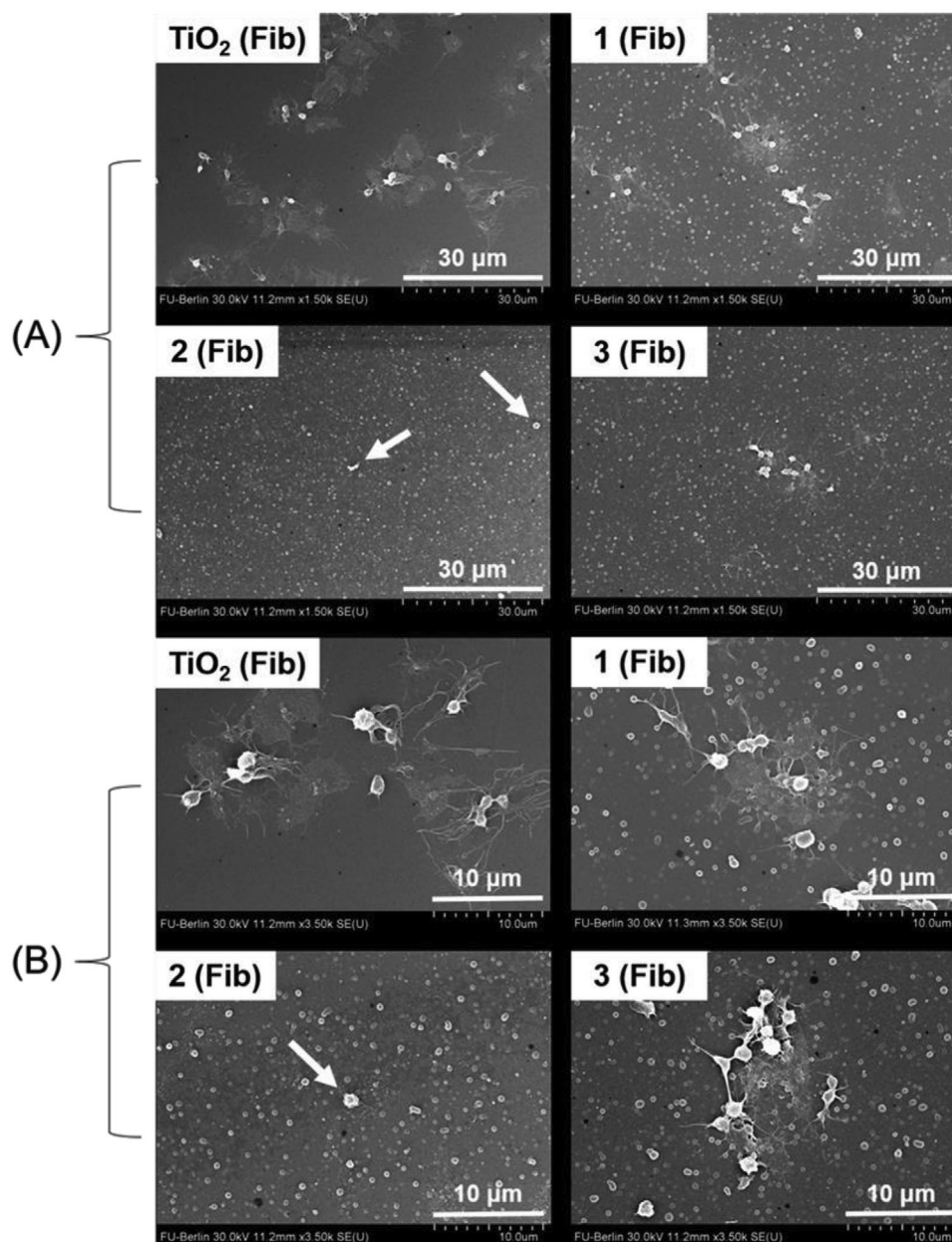


**Figure 6.** A) SEM images of the TiO<sub>2</sub> substrate (Fib), and surfaces 1 (Fib), 2 (Fib), and 3 (Fib) after incubation with PRP, at an enlargement of 1500×. B) SEM images of the same surfaces at an enlargement of 3500×. Strong activation and platelet spreading was observed on the TiO<sub>2</sub> substrate (Fib) and surface 1 (Fib). Surface 2 (Fib) showed almost no adhesion of platelets. Additionally, the settled platelets were mainly found in their inactive, spherical state. On surface 3 (Fib), fewer platelets were observed than on the TiO<sub>2</sub> substrate (Fib) and surface 1 (Fib). Nevertheless, the number of platelets seemed higher for surface 3 (Fib) than for surface 2 (Fib). Furthermore, many of the platelets observed on surface 3 (Fib) appeared in their activated morphology.

donor, ensuring that the observations resulted from the different coating types, rather than from donor-related blood variations. In total, nine sequences were performed, i.e., every substrate was tested with blood from nine different donors. Furthermore, the order in which the substrates were measured was varied in such a manner, that it was ensured that the observations resulted from the coating's surface properties, rather than from time-dependent alterations of the blood. Although large variations are common in platelet adhesion experiments,<sup>[7b]</sup> a clear reduction in platelet adhesion was observed from collagen (the

adhesion to collagen was set to 100%) > PDMS (93.4 ± 11.0% adhesion respective to collagen) > PU (80.9 ± 17.2% adhesion respective to collagen) > surface 3 (71.3 ± 22.7% adhesion respective to collagen) > TiO<sub>2</sub> (60.0 ± 27.0% adhesion respective to collagen) > surface 1 (34.7 ± 16.7% adhesion respective to collagen) > surface 2 (13.6 ± 8.2% adhesion respective to collagen) (Figure 7 and Table S3, Supporting Information). The highest surface coverage was observed for collagen, which was explained by the high affinity of the platelets' collagen receptors to the collagen substrate.<sup>[52]</sup> High platelet adsorption was also observed

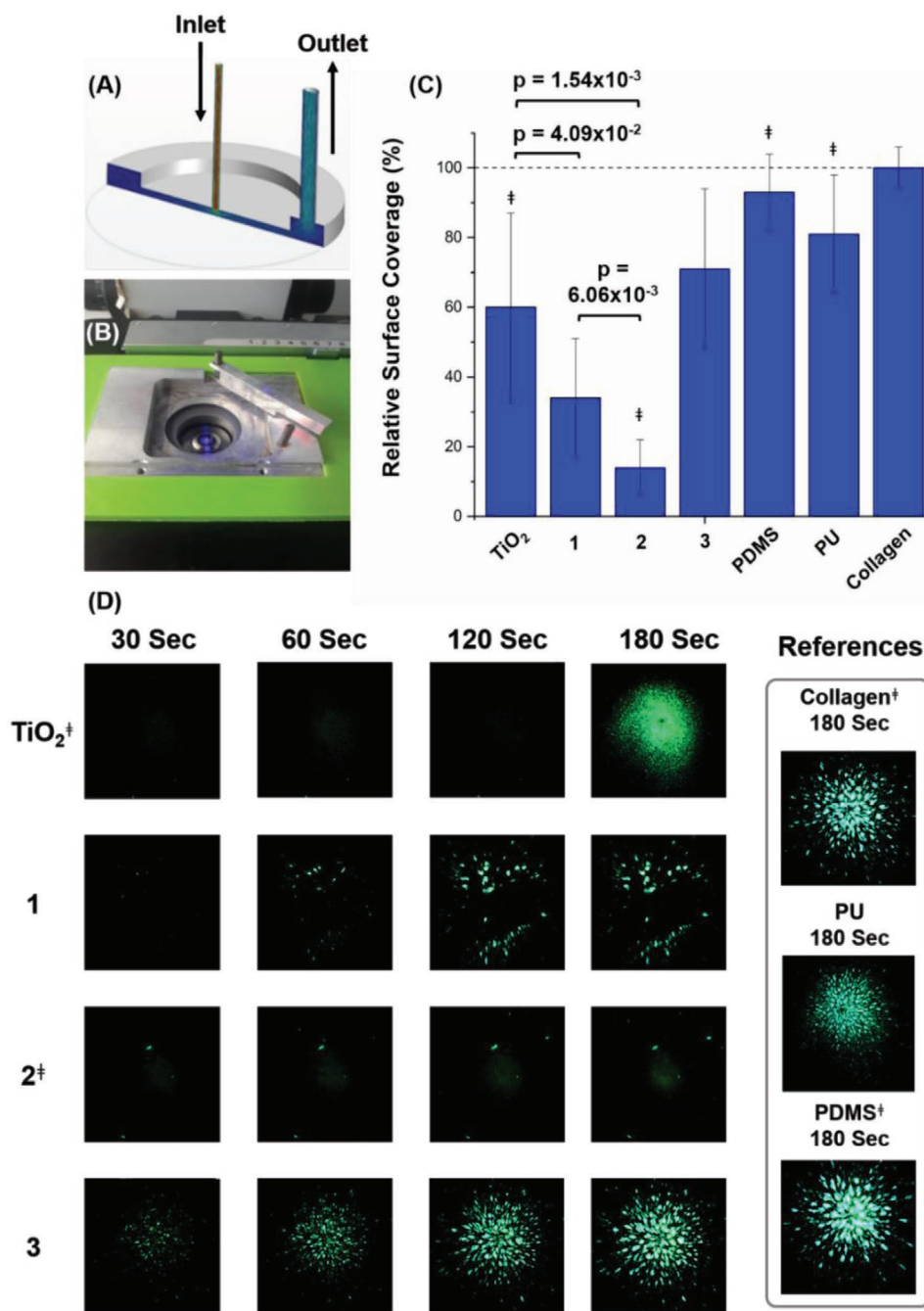


**Figure 7.** A) A computational fluid dynamics simulation of the flow within the stagnation-point flow model's flow module. Whole blood is led over the surface via the inlet at the center of the flow module. The blood leaves the system via the outlet at the edge of the flow module. For a more elaborate explanation of the flow module the reader is referred to Figure S2 in the Supporting Information. B) The holder for the flow module on top of the fluorescence microscope. The flow module is placed in the circle-structure. C) Graphical representation of the relative platelet adhesion in the stagnation-point flow model at  $t = 180$  s. All values shown are relative to the adhesion observed for the collagen positive control (i.e., the adhesion to collagen was set to 100%). The results showed that surface 2 clearly suppressed the adhesion of blood platelets. The error bars represent the standard deviation from the mean. All measurements were performed with  $n = 9$ ,  $n = 8$ . The  $p$ -values were calculated using a two-tailed  $t$ -test while assuming unequal variance. D) The fluorescence images obtained from the stagnation-point flow model for the TiO<sub>2</sub> substrate and surfaces 1, 2, and 3 at various time points. Additionally, PU and PDMS were also included in the measurements.

for the PDMS spin-coated substrate, which was explained by the hydrophobic character of this surface.<sup>[48,53]</sup> Interestingly, TiO<sub>2</sub> substrate seemed to perform well at first sight. However, single-dispersed platelets were always observed at  $t = 240$  s (Figure 7).

When compared to the TiO<sub>2</sub> substrate, higher surface coverage was observed for the PU substrate, which was explained by the more hydrophobic character of PU when compared to the TiO<sub>2</sub> substrate.<sup>[48,53]</sup> Surface 1 showed a significant reduction of

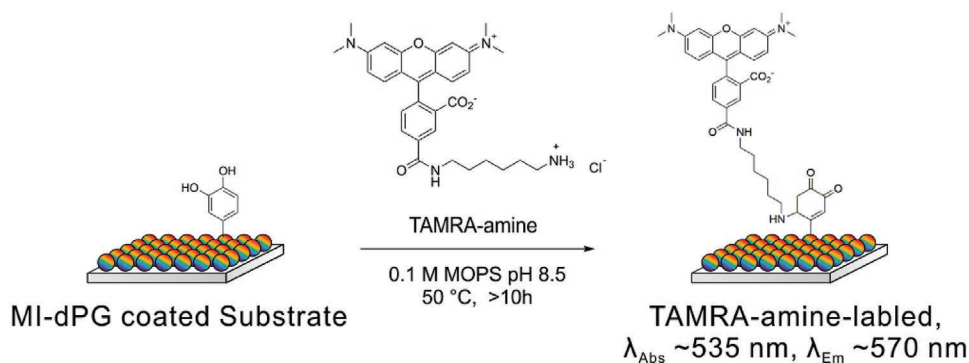


**Figure 8.** Schematic representation of the functionalization of surface 1 with TAMRA-amine.

platelet adhesion in comparison to  $\text{TiO}_2$ , which was in line with the increased hydrophilic character of the surface.<sup>[48,53]</sup> Surface 2 clearly showed the best platelet-repelling properties of all tested substrates, which was explained by the formation of a tightly bound surface water layer that prevented the adhesion of pro-coagulant protein (i.e., Fib and/or von Willebrand factor).<sup>[42]</sup> Surprisingly, surface 3 showed a relatively high surface coverage with platelets, which potentially resulted from a suboptimal PEG grafting density as a consequence of monovalent grafting of the PEG chains and the use of high molecular weight PEG (Figure 7). However, it is expected that optimization of the PEG-chain density on the MI-dPG coating will lead to surfaces that show better antifouling properties than surface 3.<sup>[17,43]</sup>

#### 4.4. Coating Applicability in VADs

To study the applicability of surface 1 on complex 3-dimensional substrates such as VADs, fluorescence studies of surface 1 postfunctionalized with a commercially available amine-functionalized fluorophore (tetramethylrhodamine (TAMRA)-amine (5-isomer)) were performed on a prototype VAD that was provided by Berlin Heart GmbH (Berlin, Germany) (Figure 8). Optimization of the TAMRA-amine post-functionalization was performed prior to the coating procedure (Figure S3, Supporting Information), in order to prevent false positives in the absence of the MI-dPG coating.

Fluorescence studies showed that the VAD prototype was successfully coated under low rotational speed (90 rotations  $\text{min}^{-1}$ ) (Figure 9). However, the fluorescence seemed more apparent at the edges of the rotor blade. These results were explained by the rotation of the rotor blade during the coating process, which might have led to a locally enhanced transport of MI-dPG and TAMRA-amine to the surface. To obtain a more homogenous distribution of the coating, the functionalization of the rotor blade was performed again under static conditions (i.e., dip coating). However, the fluorescence measurements showed similar results after introduction of the fluorophore to the MI-dPG coating. This observation was explained by the scattering of the incident light by the rounded shapes of the rotor blade. The results illustrated the limitations of fluorescence spectroscopy as a method for the control of the coating's quality. However, the combined results showed the suitability

of surface 1 in the on-line coating of VADs, i.e., the complete blood-contacting surface of a VAD was coated with MI-dPG under flow conditions, despite the aggregation and precipitation mechanism that underlies the formation of the MI-dPG coating.<sup>[37a]</sup> Based on an earlier study by our group, the further functionalization of surface 1 with IPG-*b*-OA<sub>11</sub> will lead to the formation of a highly stable protein- and cell-repelling surface within the VAD system.<sup>[37]</sup> Furthermore, the current study clearly showed the in vitro effectiveness of surface 2 in the reduction of platelet activation and adhesion under static and flow conditions. Therefore, surface 2 shows the potential to reduce biomaterial- and shear-induced thrombosis in VAD systems and other blood-contacting materials.

## 5. Conclusions

In the current work, the cell and platelet repelling properties of MI-dPG and MI-dPG post-functionalized with IPG-*b*-OA<sub>11</sub> or HO-PEG-NH<sub>2</sub> were investigated, in order to prove the applicability of the various coatings to prevent biomaterial- and shear-induced thrombosis in continuous-flow ventricular assist devices. When the adhesion and proliferation of adenocarcinomic human alveolar basal epithelial cells and chicken fibroblast cells were studied on the various substrates by fluorescent staining of the live and dead cells, it was clearly observed that the MI-dPG coating post-functionalized with IPG-*b*-OA<sub>11</sub> outperformed all other systems considering the rejection of cellular adhesion. These findings were in line with an earlier work by our group, which showed the protein and cell-repelling properties of the IPG-*b*-OA<sub>11</sub>-functionalized MI-dPG coating. High viabilities (>95%) were observed for all coating types. Subsequently, the cytotoxicity of the dissolved IPG-*b*-OA<sub>11</sub> and HO-PEG-NH<sub>2</sub> polymers towards human alveolar basal epithelial cells and chicken fibroblast cells was investigated in cell culture based experiments, in order to simulate leaching-induced cytotoxicity of these (water soluble) polymers. For the IPG-*b*-OA<sub>11</sub> polymer no cytotoxicity was observed until 5 mg  $\text{mL}^{-1}$  and 2.5 mg  $\text{mL}^{-1}$  for the A549 and the DF-1 cells, respectively. For HO-PEG-NH<sub>2</sub>, no cytotoxicity was observed until 10 mg  $\text{mL}^{-1}$  for both cell lines. It is important to notice that leaching of HO-PEG-NH<sub>2</sub> and IPG-*b*-OA<sub>11</sub> was not expected, based on the stability data presented in an earlier work of our group.<sup>[37]</sup> Human



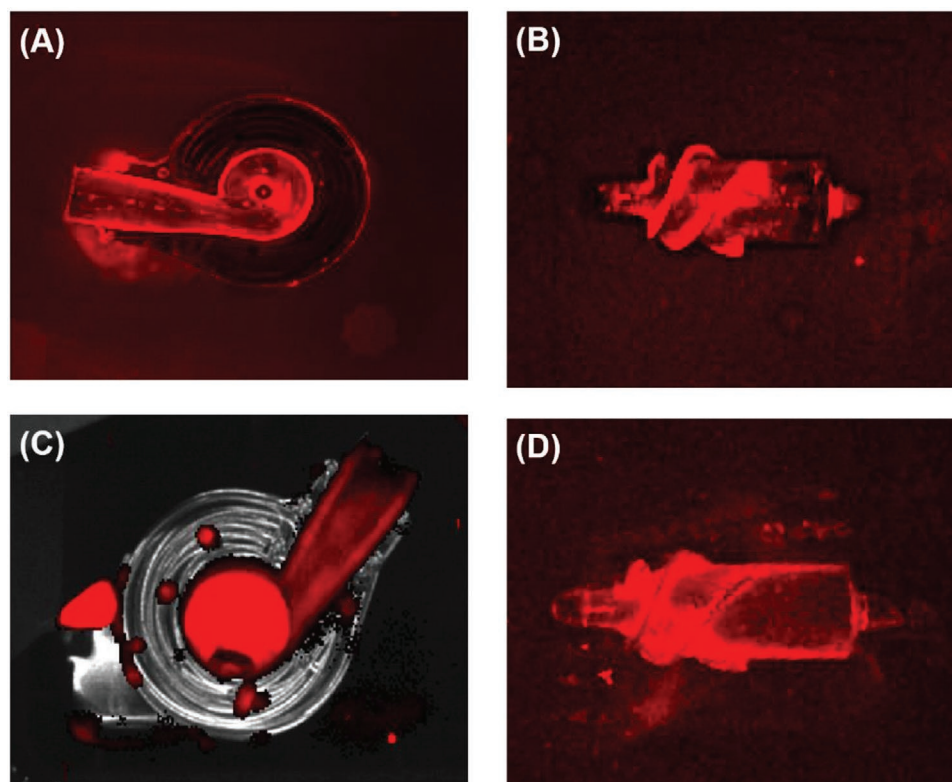


**Figure 9.** The VAD was MI-dPG coated under flow conditions and subsequently functionalized with TAMRA-amine at  $10 \mu\text{g mL}^{-1}$ . A) The picture shows the top plate of the coated VAD prototype. The illuminated channel represents the blood outlet of the VAD. B) The rotor blade of the dynamically coated VAD, showing local variations in the fluorescence intensity. C) The body of the VAD. The top plate shown in (A) is placed on top of this body to close the VAD, whereas the rotor blade shown in (B) is placed in the illuminated channel shown in (C). It was clearly observed that the blood outlet was successfully coated (right top of (C)). The VAD chamber showed bright fluorescence, which resulted from the TAMRA-amine functionalization of the MI-dPG coating in the VAD. D) The dip-coated rotor blade after TAMRA-amine functionalization. The fluorescence appeared almost equal to the fluorescence that was observed for the rotor blade that was coated with MI-dPG under flow conditions.

alveolar basal epithelial cells and chicken fibroblast cells were used in the current study, in order to show the biocompatibility of the tested coatings and their respective constituents to a broad range of cell types. Furthermore, the proliferation and adhesion of medically more relevant human umbilical vein endothelial cells on the various coatings were already investigated in an earlier study by our group.<sup>[37]</sup> It is important to notice, that in their aimed application, the coatings would not get into contact with any type of tissue (i.e., the coatings were developed as blood-contacting materials for the interior of VADs). Nevertheless, it was important that the coatings would reject cellular adhesion without being toxic to cells, as the adhesion and subsequent proliferation of cells from the bloodstream to the blood-contacting surface of the VAD could potentially lead to major complications.

When the substrate-induced activation of the complement system was analyzed by measuring the C5a levels in platelet rich plasma that had been incubated with the various coatings, no clear increase of C5a was observed in comparison to the bare  $\text{TiO}_2$  substrate. Platelet activation tests at near static conditions showed a strong activation of platelets on the fibrinogen-incubated  $\text{TiO}_2$  and MI-dPG surfaces. Less platelet activation was observed on (fibrinogen-incubated)

MI-dPG post-functionalized with monovalent PEG, and almost no activation was seen on (fibrinogen-incubated) MI-dPG that was post-functionalized IPG-*b*- $\text{OA}_{11}$ . When platelet adhesion from whole blood was investigated in the stagnation-point flow model under defined low shear-rates ( $0\text{--}180 \text{ s}^{-1}$ ), high platelet adhesion was observed for the collagen-, PDMS-, PU-, and the  $\text{TiO}_2$  substrates. The introduction of the MI-dPG coating significantly reduced the number of adherent platelets. The lowest number of platelets was clearly observed on MI-dPG post-functionalized with IPG-*b*- $\text{OA}_{11}$ . The low adhesion to the IPG-*b*- $\text{OA}_{11}$  postfunctionalized MI-dPG coating was explained by the formation of a surface hydration layer that effectively formed a barrier layer that prevented platelet adhesion.<sup>[42]</sup> Strong adhesion of blood platelets was observed for MI-dPG post-functionalized with HO-PEG-NH<sub>2</sub>, which most likely resulted from the use of a high molecular weight PEG and a suboptimal monovalent grafting of the linear polymer.<sup>[17,37,43]</sup> Finally, a VAD was coated with MI-dPG using a circulation system that allowed for the adhesion of MI-dPG while the pump was running at lower rotational speed. Subsequent visualization of the coating was achieved by the post-functionalization of the MI-dPG coating with a commercially available fluorophore.

The fluorescence data showed the successful coating of the whole interior of the VAD.

To summarize: the combined results clearly indicated that the MI-dPG coating post-functionalized with IPG-*b*-OA<sub>11</sub> showed better antifouling surface properties than TiO<sub>2</sub>, MI-dPG, and the MI-dPG coating that was post-functionalized with HO-PEG-NH<sub>2</sub>. Furthermore, no cytotoxicity and obvious complement activation were observed for any of the coatings that were topic of the current study. The IPG-*b*-OA<sub>11</sub> functionalized MI-dPG coating successfully prevented the activation of blood platelets under static conditions, and furthermore prevented the adhesion of activated blood platelets under medically relevant flow conditions. Additionally, MI-dPG was used to successfully coat a VAD under flow conditions. The combined results identify the IPG-*b*-OA<sub>11</sub> functionalized MI-dPG coating as a promising material for the effective reduction of surface blood clots in 3-dimensional, blood-contacting implant devices such as continuous-flow VADs.

## 6. Experimental Section

All materials and methods can be found in the Supporting Information.

## Supporting Information

Supporting Information is available from the Wiley Online Library or from the author.

## Acknowledgements

Dr. D. Salz (Fraunhofer IFAM, Bremen) is thanked for providing with the TiO<sub>2</sub>-coated glass substrates. The physicians, Dr. N. Al Beshar and Dr. M. Buhlaiga (Institute for Transfusion medicine, Charité-Universitätsmedizin Berlin, Berlin) are thanked for their support in regard to the blood samples. Dr. C. Schlaich (Freie Universität Berlin, Berlin) is thanked for synthesizing the used MI-dPG. S. Zürner, Dr. L. Kaufmann and Dr. V. Kunz (Berlin Heart GmbH, Berlin) are thanked for their technical support considering the VAD prototype. Dr. P. Winchester and Dr. R. Randriantsilefisoa are thanked for proofreading the manuscript. The assistance of the BioSupraMol core facility (located at the Freie Universität Berlin and supported by the Deutsche Forschungsgemeinschaft) is acknowledged for the characterization of the used polymeric materials. Finally, we would like to thank the German Ministry of Science and Education (BMBF) for financially supporting this work via the KMU-Innovativ program (under the project name "GlycoVAD").

Open access funding enabled and organized by Projekt DEAL.

## Conflict of Interest

The authors declare no conflict of interest.

## Keywords

antifouling, platelet adhesion, polyglycerol, shear-induced thrombus formation, stagnation-point flow model, ventricular assist devices

Received: February 17, 2020

Revised: June 30, 2020

Published online: September 6, 2020

- [1] M. Saini, Y. Singh, P. Arora, V. Arora, K. Jain, *World J. Clin. Cases* **2015**, *3*, 52.
- [2] E. Wilkins, L. Wilson, K. Wickramasinghe, P. Bhatnagar, J. Leal, R. Luengo-Fernandez, R. Burns, M. Rayner, N. Townsend, *European Cardiovascular Disease Statistics*, European Heart Network, Brussels **2017**.
- [3] a) J. A. Ambrose, R. S. Barua, *J. Am. Coll. Cardiol.* **2004**, *43*, 1731; b) J. Kochar, J. M. Gaziano, L. Djoussé, *Aging Dis.* **2011**, *2*, 149; c) B. A. Ference, H. N. Ginsberg, I. Graham, K. K. Ray, C. J. Packard, E. Bruckert, R. A. Hegele, R. M. Krauss, F. J. Raal, H. Schunkert, G. F. Watts, J. Borén, S. Fazio, J. D. Horton, L. Masana, S. J. Nicholls, B. G. Nordestgaard, B. van de Sluis, M.-R. Taskinen, L. Tokgözoğlu, U. Landmesser, U. Laufs, O. Wiklund, J. K. Stock, M. J. Chapman, A. L. Catapano, *Eur. Heart J.* **2017**, *38*, 2459; d) L. Anderson, N. Oldridge, D. R. Thompson, A.-D. Zwisler, K. Rees, N. Martin, R. S. Taylor, *J. Am. Coll. Cardiol.* **2016**, *67*, 1; e) P. W. Serruys, M.-C. Morice, A. P. Kappetein, A. Colombo, D. R. Holmes, M. J. Mack, E. Stähle, T. E. Feldman, M. van den Brand, E. J. Bass, N. Van Dyck, K. Leadley, K. D. Dawkins, F. W. Mohr, *N. Engl. J. Med.* **2009**, *360*, 961; f) S. K. Mulpuru, M. Madhavan, C. J. McLeod, Y.-M. Cha, P. A. Friedman, *J. Am. Coll. Cardiol.* **2017**, *69*, 189.
- [4] M. M. Givertz, *Circulation* **2011**, *124*, 305.
- [5] A. R. de Biasi, K. B. Manning, A. Salemi, *J. Thorac. Cardiovasc. Surg.* **2015**, *149*, 667.
- [6] K. Kirklin, D. C. Naftel, F. D. Pagani, R. L. Kormos, L. W. Stevenson, E. D. Blume, M. A. Miller, J. T. Baldwin, J. B. Young, *J. Heart Lung Transplant.* **2014**, *33*, 555.
- [7] a) M. Weber, H. Steinle, S. Golombek, L. Hann, C. Schlensak, H. P. Wendel, M. Avci-Adali, *Front. Bioeng. Biotechnol.* **2018**, *6*, 99; b) K. Affeld, J. Schaller, T. Wölken, T. Krabatsch, U. Kertzscher, *Biointerphases* **2016**, *11*, 029804.
- [8] D.-C. Sin, H.-L. Kei, X. Miao, *Expert Rev. Med. Devices* **2009**, *6*, 51.
- [9] K. Yamazaki, S. Kihara, T. Akimoto, O. Tagusari, A. Kawai, M. Umezaki, J. Tomioka, R. L. Kormos, B. P. Griffith, H. Kurosawa, *Jpn. J. Thorac. Cardiovasc. Surg.* **2002**, *50*, 461.
- [10] a) T. G. Kim, H. Lee, Y. Jang, T. G. Park, *Biomacromolecules* **2009**, *10*, 1532; b) S. Alibeik, S. Zhu, J. W. Yau, J. I. Weitz, J. L. Brash, *Acta Biomater.* **2011**, *7*, 4177; c) J. Lahann, D. Klee, W. Pluester, H. Hoecker, *Biomaterials* **2001**, *22*, 817.
- [11] V. V. Nikolaychik, D. M. Wankowski, M. M. Samet, P. I. Lelkes, *ASAIO J.* **1996**, *42*, 487.
- [12] N. Uriel, J. Han, K. A. Morrison, N. Nahumi, M. Yuzefpolskaya, A. R. Garan, J. Duong, P. C. Colombo, H. Takayama, S. Thomas, Y. Naka, U. P. Jorde, *J. Heart Lung Transplant.* **2014**, *33*, 51.
- [13] W. Wu, F. Yang, J. Wu, N. Aubry, M. Massoudi, J. F. Antaki, *Sci. Rep.* **2016**, *6*, 38025.
- [14] C. Cheng, S. Sun, C. Zhao, *J. Mater. Chem. B* **2014**, *2*, 7649.
- [15] R. Biran, D. Pond, *Adv. Drug Delivery Rev.* **2017**, *112*, 12.
- [16] a) M. Amiji, K. Park, *J. Biomater. Sci., Polym. Ed.* **1993**, *4*, 217; b) M. Weinhart, T. Becherer, N. Schnurbusch, K. Schwibbert, H.-J. Kunte, R. Haag, *Adv. Eng. Mater.* **2011**, *13*, B501; c) M. Wyszogrodzka, R. Haag, *Biomacromolecules* **2009**, *10*, 1043; d) T. Becher, Q. Wei, P.-L. M. Noeske, I. Grunwald, R. Haag, *Adv. Mater.* **2014**, *26*, 2688; e) L. Liu, Q. Liu, A. Singh, *Proteins Interfaces III State-of-the Art* **2012**, *1120*, 661; f) T. Mohan, R. Kargl, K. E. Tradt, M. R. Kulterer, M. Bračić, S. Hribernik, K. Stana-Kleinschek, V. Ribitsch, *Carbohydr. Polym.* **2015**, *116*, 149; g) X. Jin, J. Yuan, J. Shen, *Colloids Surf.* **2016**, *145*, 275; h) S. Jiang, Z. Cao, *Adv. Mater.* **2010**, *22*, 920; i) A. K. Epstein, T.-S. Wong, R. A. Belisle, E. M. Boggs, J. Aizenberg, *Proc. Natl. Acad. Sci. USA* **2012**, *109*, 13182.
- [17] a) W. R. Gombotz, W. Guanghui, T. A. Horbett, A. S. Hoffman, *J. Biomed. Mater. Res.* **1991**, *25*, 1547; b) L. D. Unsworth, H. Sheardown, J. L. Brash, *Langmuir* **2005**, *21*, 1036; c) K. Prime, G. Whitesides, *Science* **1991**, *252*, 1164; d) L. J. Ho, K. Jindrich,

- A. J. D. , *J. Biomed. Mater. Res.* **1989**, *23*, 351; e) K. L. Prime, G. M. Whitesides, *J. Am. Chem. Soc.* **1993**, *115*, 10714.
- [18] a) S. Han, C. Kim, D. Kwon, *Polymer* **1997**, *38*, 317; b) A. Judge, K. McClintock, J. R. Phelps, I. MacLachlan, *Mol. Ther.* **2006**, *13*, 328.
- [19] M. Imran ul-haq, B. F. Lai, J. N. Kizhakkedathu, *Biomaterials* **2012**, *33*, 9135.
- [20] C. Siegers, M. Biesalski, R. Haag, *Chemistry* **2004**, *10*, 2831.
- [21] a) C. D. Bain, E. B. Troughton, Y. T. Tao, J. Evall, G. M. Whitesides, R. G. Nuzzo, *J. Am. Chem. Soc.* **1989**, *111*, 321; b) A. Y. Fadeev, Y. V. Kazakevich, *Langmuir* **2002**, *18*, 2665.
- [22] D. Kubies, L. Machová, E. Brynda, J. Lukáš, F. Rypáček, *J. Mater. Sci.: Mater. Med.* **2003**, *14*, 143.
- [23] C. Boura, P. Menu, E. Payan, C. Picart, J. C. Voegel, S. Muller, J. F. Stoltz, *Biomaterials* **2003**, *24*, 3521.
- [24] P. Petrov, G. Georgiev D. Momekova G. Momekov, C. B. Tsvetanov, *Polymer* **2010**, *51*, 2465.
- [25] a) P. Bertrand, A. Jonas, A. Laschewsky, R. Legras, *Macromol. Rapid Commun.* **2000**, *21*, 319; b) C. Freij-Larsson, T. Nylander, P. Jannasch, B. Wesslén, *Biomaterials* **1996**, *17*, 2199.
- [26] J. H. Waite, *J. Exp. Biol.* **2017**, *220*, 517.
- [27] J. H. Waite, M. L. Tanzer, *Science* **1981**, *212*, 1038.
- [28] J. Saiz-Poseu, J. Macebo-Aracil, F. Nador, F. Busqué, D. Ruiz-Molina, *Angew. Chem., Int. Ed.* **2019**, *58*, 696.
- [29] H. Lee, N. F. Scherer, P. B. Messersmith, *Proc. Natl. Acad. Sci. USA* **2006**, *103*, 12999.
- [30] H. Lee, S. M. Dellatore, W. M. Miller, P. B. Messersmith, *Science* **2007**, *318*, 426.
- [31] R. Batul, T. Tamanna, A. Khaliq, A. Yu, *Biomater. Sci.* **2017**, *5*, 1204.
- [32] J. H. Ryu, P. B. Messersmith, H. Lee, *ACS Appl. Mater. Interfaces* **2018**, *10*, 7523.
- [33] J. Liebscher, R. Mrówczyński, H. A. Scheidt, C. Filip, N. D. Hädäde, R. Turcu, A. Bende, S. Beck, *Langmuir* **2013**, *29*, 10539.
- [34] S. Hong, Y. S. Na, S. Choi, I. T. Song, W. Y. Kim, H. Lee, *Adv. Funct. Mater.* **2012**, *22*, 4711.
- [35] Q. Wei, K. Achazi, H. Liebe, A. Schulz, P.-L. M. Noeske, I. Grunwald, R. Haag, *Angew. Chem., Int. Ed.* **2014**, *53*, 11650.
- [36] a) C. Schlaich, L. Cuellar Camacho, L. Yu, K. Achazi, Q. Wei, R. Haag, *ACS Appl. Mater. Interfaces* **2016**, *8*, 29117; b) M. Li, C. Schlaich, M. W. Kulka, I. S. Donskyi, T. Schwerdtle, W. E. Unger, R. Haag, *J. Mater. Chem. B* **2019**, *7*, 3438.
- [37] M. W. Kulka, I. S. Donskyi, N. Wurzler, D. Salz, Ö. Ozcan, W. E. S. Unger, R. Haag, *ACS Appl. Bio Mater.* **2019**, *2*, 5749.
- [38] M. Gervais, A.-L. Brocas, G. Cendejas, A. Deffieux, S. Carlotti, *Macromolecules* **2010**, *43*, 1778.
- [39] A. Sunder, R. Hanselmann, H. Frey, R. Mülhaupt, *Macromolecules* **1999**, *32*, 4240.
- [40] S. P. Pujari, L. Scheres, A. T. M. Marcelis, H. Zuilhof, *Angew. Chem., Int. Ed.* **2014**, *53*, 6322.
- [41] I. F. Amarai, A. L. Cordeiro, P. Sampaio, M. A. Barbosa, *J. Biomater. Sci., Polym. Ed.* **2007**, *18*, 469.
- [42] S. Chen, L. Li, C. Zhao, J. Zheng, *Polymer* **2010**, *51*, 5283.
- [43] S. J. Sofia, V. Premnath, E. W. Merrill, *Macromolecules* **1998**, *31*, 5059.
- [44] D. Fisher, Y. Li, B. Ahlemeyer, J. Krieglstein, T. Kissel, *Biomaterials* **2003**, *24*, 1121.
- [45] T. E. Mollnes, *Vox Sang.* **1998**, *74*, 303.
- [46] J. Hed, M. Johansson, M. Lindroth, *Immunol. Lett.* **1984**, *8*, 295.
- [47] M. I. Jones, I. R. McColl, D. M. Grant, K. G. Parker, T. L. Parker, *J. Biomed. Mater. Res.* **2000**, *52*, 413.
- [48] B. Sivaraman, R. A. Latour, *Biomaterials* **2010**, *31*, 832.
- [49] W. Wang, Z. Zheng, X. Huang, W. Fan, W. Yu, Z. Zhang, L. Li, C. Mao, *J. Biomed. Mater. Res., Part B* **2017**, *105*, 1737.
- [50] K. Affeld, S. Stefansdottir, J. Schaller, U. Kertzschner, *Biomed. Tech.* **2014**, *59*, 11.
- [51] a) M. Kütting, J. Roggenkamp, U. Urban, T. Schmitz-Rode, U. Steinseifer, *Expert Rev. Med. Devices* **2011**, *8*, 227; b) B. H. Shin, B. H. Kim, S. Kim, K. Lee, Y. B. Choy, C. Y. Heo, *Biomater. Res.* **2018**, *22*, 37.
- [52] D. E. Roberts, A. McNicol, R. Bose, *J. Biol. Chem.* **2004**, *279*, 19421.
- [53] W. Norde, *Macromol. Symp.* **1996**, *103*, 5.